Localized oscillations and Fraunhofer diffraction in crystalline phases of a monolayer

Julián Galvan-Miyoshi and Salvador Ramos
Instituto de Física, UNAM, P.O. Box 20-364, D.F. 01000, México

Jaime Ruiz-Garcia
Instituto de Física, UASLP. A. Obregón 64, San Luis Potosí, S.L.P., 78000, México

Rolando Castillo[a)]
Instituto de Física, UNAM, P.O. Box 20-364, D.F. 01000, México

(Received 2 March 2001; accepted 16 August 2001)

Localized oscillations present in the crystalline phases of the heneicosanoic acid Langmuir monolayer were studied in detail. They appear like blinking interference rings, when observed with Brewster angle microscopy. Monolayers with localized oscillations were transferred on mica to be characterized by atomic force microscopy. We found granules produced by the expulsion of matter from the monolayer. However, these granules are too short to produce Newton's rings; the common belief of the origin of the interference rings in the field of Langmuir monolayers. The analysis of the light intensity distribution and the sizes of the rings are consistent with Airy patterns produced by Fraunhofer diffraction due to the reflected light from the multilayer granules. The origin of the blinking of these patterns is still unclear. © *2001 American Institute of Physics.*
[DOI: 10.1063/1.1409401]

I. INTRODUCTION

Amphiphilic molecules that are insoluble in water can form monolayers at the air–water interface, usually called Langmuir monolayers (LMs). The most common way for studying these monolayers has been through the measurement of surface pressure isotherms $\Pi(A,T)=\gamma_0(T)-\gamma(A,T)$, where T is the temperature, A is the area/molecule, γ and γ_0 are the surface tensions of the LM and of pure water, respectively. However, the use of new techniques, such as grazing incidence x-ray diffraction, polarized fluorescence microscopy (PFM), and Brewster angle microscopy (BAM), have contributed to obtain a general picture of the fatty acid LM, as well as, the structure of their phases.[1] At very low surface densities, an amphiphilic monolayer behaves as a two-dimensional gas. A first-order phase transition from the gas phase to a liquid-expanded phase is observed upon compression of the monolayer. This phase is isotropic and molecules are tilted, although, this tilting is not correlated.[2] A second phase transition to a liquid condensed state is observed upon further compression of the monolayer. Actually, the liquid condensed phase is made up of a variety of mesophases, which show distinct molecular tilt. In addition to mesophases, crystalline phases have been found with a quasi-long-range positional order. They are *CS* and L_2'' phases, which are centered rectangular with herringbone order. L_2'' is a two-dimensional crystal with a *NN*-tilt[3] and *CS* is untilted.[3–7] Textures of condensed phases and the precise coexistence lines between phases have been obtained mainly using PFM and BAM.[8–11] At very high pressures, when A or Π reach a limiting value beyond which the monolayer cannot be further compressed, all phases collapse in multilayers. The loss of material and, hence, the loss of interfacial area can occur in several ways. LMs can fracture and break as it is usually seen with BAM in *S* and *CS* phases; buckle at constant area,[12] form folds or ridges,[13] etc. The different ways of collapse, as well as, the details of the multilayering process are unknown. However, some similarities have been suggested.[14]

In crystalline phases of the heneicosanoic acid (C_{21})LM, it has been observed with BAM, something that reminds us of interference rings that are blinking. They suddenly appear and completely disappear in the same place on the monolayer, for that reason, they have been named as *localized oscillations* (LO).[11] Apparently, this is a different form to start the formation of multilayers, where material is locally ejected from the monolayer, quite below the so-called "collapse pressure." Here, we present a series of experiments to show the behavior of these LO in monolayers that are prepared in different conditions. Atomic force microscopy (AFM) observations of transferred monolayers on mica when the LO are present were also studied. In addition, we present a model that explains the origin of the interference patterns, as well as a series of experiments to support that model. However, although many of the features of these LO could be understood with the model, the reason of why these interference patterns are blinking is still unclear.

II. EXPERIMENT

C_{19}(99%), C_{21}(99%), C_{22}(99%), and C_{23}(99%) were purchased from Aldrich (Milwaukee, U.S.A.), and C_{20}(99%) from Merck (Darmstadt, Germany). All of them

a)Author to whom correspondence should be addressed. Electronic mail: rolandoc@fenix.fisica.unam.mx

were used without any further purification. With the aid of a spreading solution, fatty acids were spread onto a subphase of ultrapure water (Nanopure-UV) at $p\mathrm{H}=2$. The spreading solution was made with chloroform (HPLC; Aldrich, Milwaukee, U.S.A.). HCl (Merck, Mexico) was used to modify pH.

All monolayers were prepared on a computerized Nima LB trough (TKB 2410A, Nima Technology Ltd., England) using a Wilhelmy plate to measure the Π. The trough is isolated from vibrations using a pneumatic tube incorporated into a steel base. All experiments were carried out in a dust-free environment. Temperature in the trough was kept constant with the aid of a water circulator bath (Cole-Parmer 1268-24, U.S.A.).

AFM observations were performed with a Nanoscope IIIa (Digital Instruments, CA, U.S.A.), working in tapping mode using standard silicon nitride canterlivers. The BAM observations were performed using a BAM1 (Nanofilm Technologie GmbH, Germany) with a spatial resolution of $\approx 4\ \mu$m. The interface where the monolayer is deposited, is illuminated at the Brewster incidence ($\sim 53°$) with a p-polarized beam coming from a He–Ne laser. A lens receives the reflected light. Afterwards, the reflected light is sent to a polarization analyzer with the aid of a mirror that makes a specular inversion of the image. Finally, the polarization-analyzed light is received by a CCD video camera to develop an image of the monolayer.

BAM is based on the study of the reflected light coming from an interface illuminated at the Brewster angle, by a p-polarized laser beam.[15,16] When the angle of incidence of this beam is at the Brewster angle, the reflected intensity is a minimum for a real interface, which has a transition region where the refractive index changes smoothly from one value to another. The reflected intensity at this angle is strongly dependent on the interfacial properties, mostly when a monolayer is involved in the interface. The reflectivity has three origins:[16] (a) the thickness of the interface; (b) the roughness of the real interface due to thermal fluctuations; (c) the anisotropy of the monolayer. Reflected light is a function of the orientation of the molecules in monolayer domains. In tilted phases, the anisotropy is relatively strong producing enough light reflection, to make quite visible the mosaic of textures due to tilted domains in different directions. In untilted phases with rectangular lattice symmetry, textures are also visible, but with much less contrast. On the other hand, multilayer structures reflect very large quantities of light as compared with monolayers.

III. RESULTS AND DISCUSSION

A. BAM observations of monolayers

LO are observed in the crystalline phases of the C_{21} monolayer with BAM (see Fig. 1). They are like circular interference patterns, which are blinking, i.e., they suddenly appear and completely disappear in the same place of the monolayer. LO can be observed along the monolayer at several parts of the field of view of the Brewster angle microscope. In addition, it is common to observe interference patterns that are not blinking. This kind of defect is common in

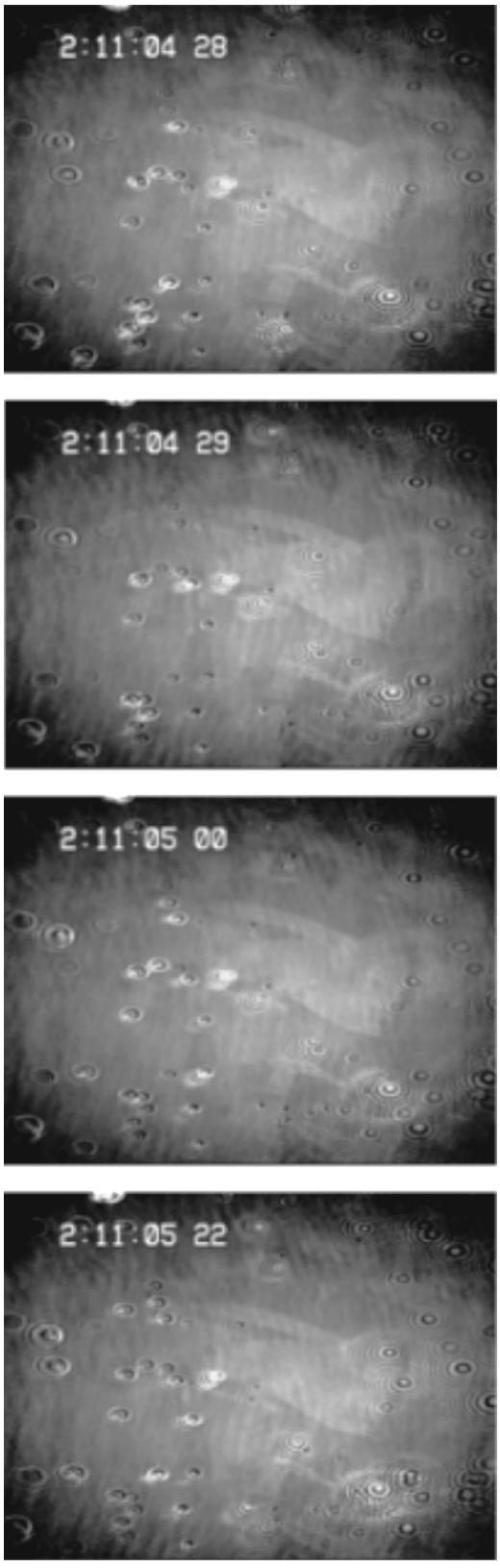

FIG. 1. BAM images of crystalline phases of the C_{21} monolayer, showing interference rings that suddenly appear and disappear in the same place on the monolayer, as well as, fixed interference patterns. They were obtained from our VCR tape observation records. They correspond to four different images coming from the same area of observation in the monolayer. In all figures, the horizontal breadth corresponds to $\approx 850\ \mu$m. Numbers indicate the elapsed time (h:min:s s/30).

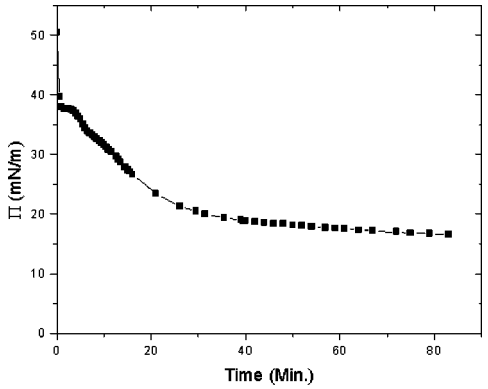

FIG. 2. Relaxation of Π as a function of time when LO are present.

condensed phases of monolayers, at temperatures below 10 °C. The LM community has colloquially named these fixed patterns as Newton rings. The elapsed time between the successive first three images in Fig. 1 is ≈ 1/30 s and the fourth was taken ≈ 22/30 s after the third one. In these images, some interference patterns are seen in one of the images, but not in the others. The area where our microscope is in focus is just a vertical strip and it is not very wide. In the examples given in Fig. 1, the microscope is in focus close to the center of the images, where some phase domains are clearly seen. Going to the right from the focused area, the domains are little bit out of focus and the interference patterns seem to be larger. On the contrary, going to the left from the area that is in focus, the patterns are not seen sharp. Thus, a fixed or a blinking pattern is larger at the right, and its size decreases as we move close to the focused area. At the center of the area that is in focus, the patterns change their white center to a small black one. As we move to the left away from the focused area, the patterns are out of focus, as well as that part of the image. The apparent size of the patterns ranges from 50 to 100 μm, as seen in the monitor. LO also appear in the crystalline phases of C_{20} (~2 °C), and C_{22} (2.4–3.3 °C), although not in a big number. In the latter, we found them close to big defects and near to the collapse. We did not find LO neither in C_{23} nor in C_{19}. For this reason, our report is based mainly on the C_{21} LO.

Lateral pressure changes when the interference patterns are blinking. Figure 2 shows a typical curve of the relaxation of Π as a function of time, when LO are present. The larger the pressure drops the larger the number of LO in the monolayer. BAM reveals the formation of typical mountain-shaped multilayer structures, as pressure goes down after long periods of blinking. However, when LO are just starting, it is possible to see in some cases, the formation of an irregular white domain at the place where the interference rings are blinking, suggesting that a multilayer domain is starting to grow there. The oscillations remain for a long time until pressure relaxes to values close to ~12 mN/m. Below this value, LO disappear or remain as fixed interference patterns. Π continues its relaxation continuously to values close to 0 mN/m after 24 h, probably to reach the equilibrium spreading pressure. We were unable to measure a characteristic time of blinking for the LO. We have associated a ''period of oscillation'' to the blinking. We found LO

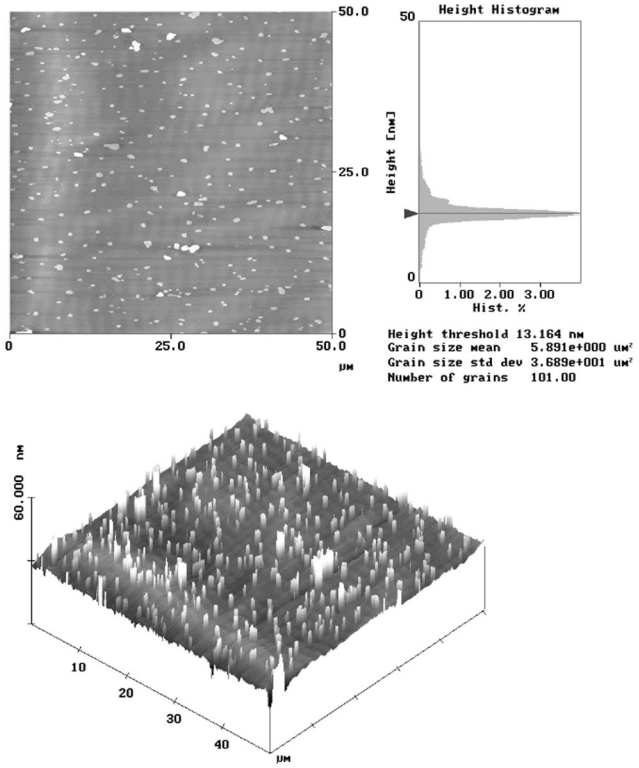

FIG. 3. Images of a transferred monolayer on mica, obtained by AFM, when there is a high population of LO.

with very different periods of oscillation, some of them have a period of 1–2 s and others have a period less than a fraction of a second. However, it is not difficult to find very short periods of oscillation, in the range of 1/15 s. We followed some of the rapid oscillations for 10 s, and we noticed that the period of blinking is not regular.

LO start at low temperature (~2–6 °C), as well as at low pressure (~12 mN/m) compared to the collapse pressure, which is around ~60 mN/m. However, as the pressure is increased, the number of oscillations sites increases notoriously. Compressions at very slow rates (30 cm^2/min) present less number of LO than in more rapid compressions (100 cm^2/min). If crystalline phases are reached by decreasing temperature slowly, starting from a more fluid phase, like *LS*, LO never show up. Although, some fixed interference rings remain. When a monolayer is deposited onto a cold subphase (2–3 °C), compressed up to Π = 25 mN/m (~24 $Å^2$/molecule), and subsequently, the temperature is increased slowly up to 15.5 °C (2 h), maintaining fixed the Π, there are too many oscillations at the beginning. However, as the temperature increases, the number of localized oscillations decreases, as well as, the area of the monolayer, i.e., there is a loss of molecules in the monolayer. LO completely disappear when we leave the crystalline phases.

B. AFM observations of transferred monolayers

Monolayers with a high population of LO were transferred over mica (transfer rate = 1 mm/min) and observed with an atomic force microscope (AFM). Figure 3 presents an example of an AFM image of a transferred monolayer. As a general feature, we found a homogeneous surface covered

with granules with sharp edges, but with an irregular round contour, seeming like irregular disks. A typical grain size is of the order of 5 μm, and typical heights are in the range of 0.013–0.018 μm. Variations in grain size are more common than variation in height. Grain size was more dependent on the specific procedure of monolayer preparation. It is common to see a few grains with sizes larger than the average, $\approx$10–15 μm. We never found grain heights much larger than the average value. In very few cases, there were some grains higher than 0.1 μm, but they never reached 0.2 μm. These results agree with the event of expelling of matter out of the monolayer, as described above. Probably, with a mechanism much more complicated that those given for ridge formation by Ries *et al.*,[13] or the nucleation, growth, and collision theory of Vollhardt.[17,18] In general, the irregular disks over the monolayer are uncorrelated and they are formed by several layers of C_{21}. The density of granules in the AFM image does not necessarily correspond to the density of interference patterns of Fig. 1, because they were obtained from different areas in the monolayer. However, big granules seem to appear sometimes in clusters.

C. Model for the sources of the interference patterns

The results presented above suggest that during a normal compressing process, there is not enough time for a proper relaxation in crystalline phases of the monolayer. Thus, an adequate matching of the different order parameters at grain boundaries of the phases does not occur. Therefore, there are big areas with a high density of defects and consequently, stress and energy are concentrated in those areas. The monolayer apparently relaxes expelling matter out of the monolayer. The AFM results suggest that BAM is able to detect the formation of the granules, product of the expulsion of matter from the monolayer. Nevertheless, why do we see something like interference rings? A common belief is that they are the result of light interference. This would be the case in a thick film, where some portion of the light is refracted and another reflected, at the surface of the thick film. The refracted light is subsequently reflected in the next lower boundary (water subphase). An interference pattern is obtained, when both portions of light are mixed because of the difference in optical path. However, this could not be the case for the granules or irregular disks found in the transferred monolayer with the AFM. Here, the disk height could not allow interference when illuminated with light in the way just mentioned, because of the granules are too short for the wavelength of light. There is not enough optical path difference, when a wavelength $\lambda = 632.8$ nm is used to illuminate the monolayer with the Brewster angle microscope.

The mesoscopic granules made of few amphiphilic molecule layers ($\sim$5–9), laying over the monolayer will reflect relatively large quantities of light. In contrast, the monolayer will be working as an almost opaque screen, because of its relative low reflectivity. This situation is equivalent to that formed by a black screen with an aperture, where light is coming from below of the black screen, at the Brewster angle, and observed in the far field. In this situation, Fraunhofer diffraction must be observed, because of the finite size

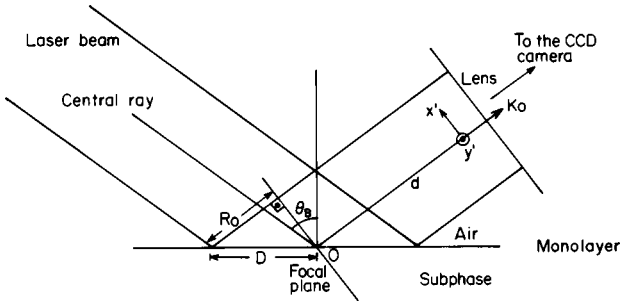

FIG. 4. The illuminated interface with the *p*-polarized beam the central ray arriving to the interface at the Brewster angle, the reflected beam, the lens, and its focal plane.

of the light source (aperture or reflecting disk). Therefore, in a first approximation, we will model the mesoscopic granules laying on the monolayer as circular disks lying on a relative opaque screen, where the reflected light coming from the disks is much more intense than the reflected light coming from the monolayer. The light intensity distribution for a circular diffracting aperture or for a disk, of radius *s*, reflecting light can be calculated using the formula for diffracted electric fields coming from the Kirchhoff vector integral formula, in the Smythe–Kirchhoff approximation,[19]

$$\frac{\langle I(R,\theta,\phi)\rangle}{P_i} = \frac{\cos\theta_B (ks)^2}{4\pi R^2}[\cos^2\theta + \sin^2\theta\cos^2\phi] \times \left[\frac{2J_1(ks\xi)}{ks\xi}\right]^2. \quad (1)$$

This interference distribution is known as the Airy pattern, when $\theta_B = 0$. Here, R,θ,ϕ are the polar coordinates for a point of observation far away from the disk, P_i is the total power normally incident on the disk, θ_B is the Brewster angle, $\xi = \sqrt{\sin^2\theta_B + \sin^2\theta - 2\sin\theta_B\sin\theta\cos\phi}$ and J_1 is a Bessel function. This approximation is not valid for $ks \leqslant 1$. The observed distribution, in the direction of the reflected ray (direction of observation of the microscope), can be obtained through an expansion of Eq. (1).[19] The observed distribution relative to the maximum intensity on an observation plane can be written as

$$I_{\text{relative}}(x',y') = \left\langle \frac{I(x',y')}{I(\theta_B,0)} \right\rangle = \left[\frac{2J_1(ks\rho/R)}{ks\rho/R}\right]^2, \quad (2)$$

where

$$\rho^2 = \frac{x'^2}{\sec^2\theta_B} + \frac{y'^2}{\csc^2\theta_B},$$

where x' is defined in the incidence plane and y' perpendicular to the incidence plane, on the plane of observation $X'Y'$ (see Fig. 4). The relative intensity distribution (2) starts at a maximum intensity equal to 1, in the direction of observation and decays as the Airy pattern. This distribution must have constant values in the plane of observation $(X'Y')$ at the geometrical loci where x' and y' vary in such a way that $\rho^2 = \text{constant}$, i.e., at ellipses. Therefore, the observed distribution would be a deformed Airy pattern, since

TABLE I. Calculated and experimental values for the semimajor axis ratios for white and black rings and percent deviation from the experimental values.[a]

		White rings $(a'_n/a'_1)\pm\sigma$			Black rings $(a_n/a'_1)\pm\sigma$	
n	Theory	Experiment	%	Theory	Experiment	%
1	1	1	0	0.74	0.53 ± 0.05	38.0
2	1.64	1.75 ± 0.11	6.5	1.36	1.42 ± 0.08	4.3
3	2.26	2.40 ± 0.19	5.5	1.98	2.10 ± 0.15	5.9
4	2.88	2.94 ± 0.25	2.1	2.59	2.67 ± 0.21	3.1
5	3.5	3.44 ± 0.31	1.6	3.21	3.21 ± 0.28	0.1
6	4.11	3.98 ± 0.36	3.2	3.82	3.74 ± 0.34	2.1
7	4.73	4.46 ± 0.43	6.0	4.43	4.24 ± 0.41	4.6

[a]A set of 33 randomly chosen patterns coming from different monolayer preparations were used to obtain the averages.

the rings where intensity is zero or a secondary maximum are elliptical in shape. Using Eq. (2), the semimajor axis of the central disk, of the different n-black rings, and of the n-white rings can be written as

$$a_n=\frac{J_1(\alpha_{1n})}{\pi\cos\theta_B}\frac{R\lambda}{2s} \quad \text{and} \quad a'_n=\frac{J_2(\alpha_{2n})}{\pi\cos\theta_B}\frac{R\lambda}{2s}. \tag{3}$$

In these equations, α_{mn} are the zeroes for the Bessel function J_m. As a consequence of expressions (3), a test of the model can be given measuring the semimajor axes in the observed rings of a pattern. This test could be a very precise, if some internal distance in the pattern is taken as a reference distance. The Brewster angle microscope introduces magnification factors. An optical one, which only depends on the distance from the pattern to the focal plane (R_0 in Fig. 4), and others that comes from the instrumentation. The latter ones make the images larger in the plane of incidence (parallel to X'), than in the direction perpendicular to the plane of incidence (parallel to Y'). All amplification factors must be approximately the same for each ring in a given pattern. Therefore, if semimajor axis ratios in a pattern are measured, taken one specified semimajor axis as a reference, then the amplification factors would cancel and there is no need to calculate them explicitly. Here, we used ratios of the semimajor axis for each ring (black or white) to the semimajor axis of the first white ring. Table I presents calculated values for the semimajor axis ratios of the first seven white and black rings in a pattern, calculated by Eqs. (3), as well as, average measurements for the same semimajor axis ratios made on electronically amplified BAM images. The agreement is quite good, since deviations from the calculated values are in the range of a few percent, except for the first black ring. For the first black ring, we observed that the perimeter of several central white disks is not perfect circular. Shades of gray suggest polygonal shapes circumscribing the disks. This made difficult the determination of where to take the end of the central disk and consequently, the central part of the first black ring. We believe that this effect is because the actual granules are not circular, as shown by the AFM images, and in the boundary comes some information about the actual shape of the reflecting disks. For the seventh ring, the statistics is not so good because in some of the patterns it was not possible to measure this ring. Another important outcome was that the blinking patterns, as well as the fixed patterns gave the same semimajor axis ratios results. This suggests that around a fixed pattern the expulsion of matter has ended, probably because the monolayer has locally relaxed.

We measured the brightness intensity for blinking patterns. The levels of intensity to be analyzed are quite different in magnitude. The intensity of the central white disk in an Airy pattern is two orders of magnitude larger than the intensity of the first white ring. Therefore, this is a semiquantitative test because the capability of the microscope for this kind of light intensity measurements is limited. An example of the brightness intensity measurements is presented in Fig. 5. In this figure, we present the intensity along a line crossing the pattern horizontally in the middle. The central disk is quite intense reaching the white level saturation. In the next rings, although the base line is not horizontal, the brightness intensity of the peaks decreases as the ring number increases. However, the intensity of the secondary maxima has the same order of magnitude, as expected from our calculations. Digitalizing calculated patterns obtained with Eq. (1), and

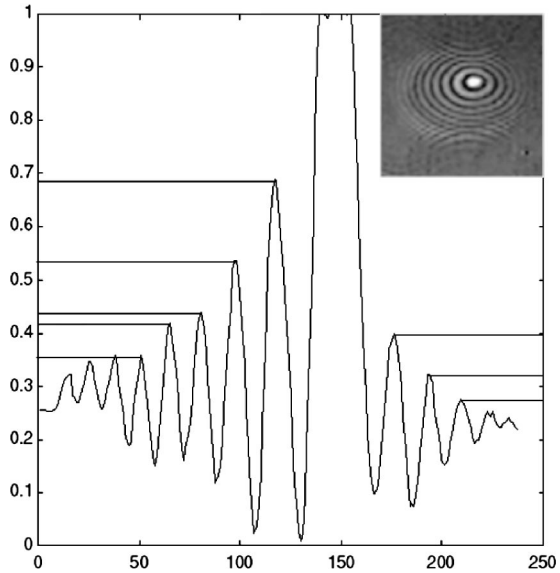

FIG. 5. The brightness intensity distribution, in arbitrary units, along a line crossing a pattern (inset) horizontally in the middle. The brightness was obtained on an electronically amplified BAM image of a pattern using a normalized gray scale for each pixel (0 for black and 1 for white).

treating the electronic image in the same way as in Fig. 5, we obtained a similar figure. A central peak quite intense saturating the white level, and the first four white peaks present intensity maximum values of 0.7, 0.5, 0.42, and 0.37, using the same arbitrary units as those used for Fig. 5. We analyzed 24 patterns and 75% gave the same results. For the remaining patterns, the central peak is not so high or the base line is nonuniform, although the structure of the patterns is the same.

The light intensity distribution was calculated using Eq. (1) for $\theta_B = 53°$. Figure 6(a) presents a calculated light intensity distribution pattern for a disk of a radius $s = 15\ \mu$m located at a specific position from the focal plane, just as it would be observed in the monitor of our microscope; with R_0 (Fig. 4) the optical amplification factor was evaluated. The instrumental amplification factors were determined from direct observation of a micrometer scale on the microscope screen monitor. Figure 6(b) presents a pattern for a LO taken from our video recordings, at the same distance from the focal plane as in Fig. 6(a). Both Figs. 6(a) and 6(b) are approximately in the same scale. In Fig. 6(c), we present the superposition of the calculated and the actual pattern presented in Figs. 6(a) and 6(b). The fitting is quite remarkable. However, a remark must be made. The disk radius used in the calculation (15 μm) is larger than the mean grain size obtained by AFM observations of the transferred monolayers. If we use a smaller radius, the intensity of the reflected light is also smaller, and the patterns are deformed (they are quite eccentric); the smaller the radius the more deformed pattern. This is because the incoming light at the Brewster angle sees the disk as shorter in the plane of incidence that is perpendicular to it. Diffraction is larger in the plane of incidence. Although, small disks produce diffraction, their patterns are of so low intensity that our BAM do not see them. Probably, we are observing the diffraction from the larger discs, the same kind of large granules seen in the AFM images.

As mentioned above, patterns are large and well defined at the right of the area that is in focus. Patterns are smaller and the white center changes to a black center in the area in focus. When the patterns are to the left, the definition of the patterns is lost. These events can be easily explained with the aid of Fig. 4. BAM images are mirror inverted. Therefore, those areas on the screen that are seen at the right side of the focused area are actually at the left of the focal plane (see Fig. 4) and vice versa. Thus, patterns that are not in focus correspond to patterns that are at the right of the focal plane and cannot be seen in focus. On the contrary, the well-defined patterns are at the left of the area that is in focus and in addition, far from the focal plane. From this plane, the Fraunhofer diffraction patterns are taken by the lens to be focused in the CCD camera. In particular, the Fresnel number[20] ($N_F = s^2/\lambda R_0$) calculated from the actual sources, i.e., the reflecting granules giving large patterns to the focal plane is ≈ 0.015. As we move the BAM to leave the patterns in the area that is in focus, i.e., at the focal plane of Fig. 4, the diffraction patterns are taken very close or at the finite source of light. Therefore, the observed patterns must be Fresnel diffraction patterns. One important characteristic of a Fresnel pattern is to have a black center. In this situation, the Fresnel number as expected is quite high, since R_0 is very small.

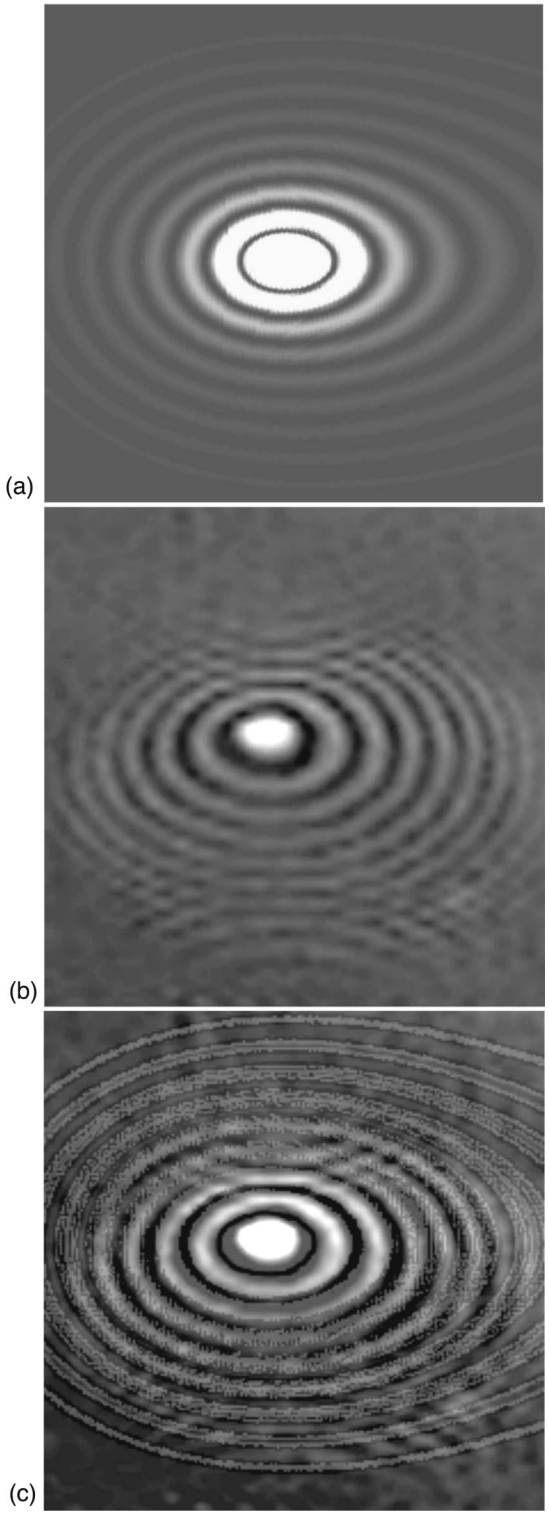

FIG. 6. (a) Calculated light intensity distribution pattern for a disk of a radius $s = 15\ \mu$m, as it would be observed in the monitor of our Brewster angle microscope. A gray scale was used, where the brighter area, the greater the value of the intensity distribution. (b) A pattern for a LO taken from our video recordings at the same place in the monolayer where (a) was calculated. (c) Superposition of the calculated and the actual patterns given in (a) and (b).

IV. CONCLUDING REMARKS

We have shown that multilayer granules are formed when LO are present. The number of observed LO can be modified by annealing the monolayer, suggesting that the appearance of LO depends on the density of defects in the LM. Our results are consistent with the fact that the ring patterns observed in monolayers are Airy patterns, due to Fraunhofer diffraction produced by the reflected light coming from multilayer granules. Notwithstanding the success of our model for explaining the optical nature of the patterns, it does not help to understand the origin of the blinking. Several possibilities can be considered: (1) LO could be a process of successive steps of expulsion of matter, granule formation, and discontinuous growing using the subsequent expelled material. In this way, the diameter of the granules would change after each successive expulsion. The granules formed and reformed could cause the blinking. They would reflect light discontinuously due to the abrupt changes during the reformation of the granules. However, it is difficult to explain why this process has to be mesoscopically discontinuous to see patterns appearing and disappearing, in particular, when the period of oscillation is very short. (2) It can be considered that even when the disks are formed, their lattice organization is fluctuating trying to reach the most stable configuration. In the same way, the dielectric constant and the index of refraction are fluctuating. This also gives rise to reflectivity fluctuations, which could be the responsible of the blinking. (3) There are few but very clear examples of grain wobbling. Here, patterns change their intensity without completely disappearing. They seem like disks swinging or wobbling. One explanation could be that in areas with a high density of defects and consequently, stress and energy, matter is sent out from the monolayer producing big perturbations there, in such a way that the granules that are upon the monolayer are wobbling. In some cases this swinging could be not so big, producing the kind of wobbling observed with BAM. Nevertheless, in other cases this wobbling could make that the reflected light missed the CCD camera giving the impression that they are blinking.

The blinking of interference patterns seems to be related to abrupt expulsion of material out of the monolayer in areas with high stress, although, the actual mechanism is not known. The fixed Airy patterns along the monolayer that apparently do not change are probably granules formed during previous periods of expulsion of matter, which ended when the monolayer relaxed locally. If this scheme is right, a procedure could be developed for observing stress relaxation in crystalline phases, through the measurement of distribution and frequency of blinking patterns and the way they become fixed along the monolayer. However, we need to understand the mechanisms of how 3D structures are formed and how they are related to pattern blinking to take advantage of them. Several directions of research could be followed. Imaging the diffuse light scattered from monolayers[21] could reveal the surface roughness and the growing of grains that could serve as precursors of monolayer collapse *in situ*, during pattern blinking periods. Brewster angle autocorrelation spectroscopy[22] could be used to obtain mean characteristic times for pattern blinking in specific domains. These characteristic times must be related to the mechanism of expulsion or formation of the multilayer granules. Area relaxation analysis[17,18] could be of help to correlate the mechanism of formation of the 3D structures.

ACKNOWLEDGMENTS

The authors acknowledge the partial support of DGAPAUNAM Grant No. IN103598 and CONACYT 27513-E grant, and the help of M. A. Valdes.

[1] V. M. Kaganer, H. Möhwald, and P. Dutta, Rev. Mod. Phys. **71**, 779 (1999).
[2] Th. Rasing, Y. S. Shen, M. W. Kim, and S. Grubb, Phys. Rev. Lett. **55**, 2903 (1985).
[3] B. Lin, M. C. Shih, T. M. Bohanon, G. E. Ice, and P. Dutta, Phys. Rev. Lett. **65**, 191 (1990).
[4] D. K. Schwartz, M. L. Schlossman, and P. S. Pershan, J. Chem. Phys. **96**, 2356 (1992).
[5] M. L. Schlossman, D. K. Schwartz, P. S. Pershan, E. H. Kawamoto, G. J. Kellogg, and S. Lee, Phys. Rev. Lett. **66**, 1599 (1991).
[6] K. Kjaer, J. Als-Nielsen, C. A. Helm, P. Tippman-Krayer, and H. Möhwald, J. Phys. Chem. **93**, 3200 (1989).
[7] T. M. Bohanon, B. Lin, M. C. Shih, G. E. Ice, and P. Dutta, Phys. Rev. B **41**, 4846 (1990).
[8] D. K. Schwartz and C. M. Knobler, J. Phys. Chem. **97**, 8849 (1993).
[9] S. Rivière-Cantin, S. Hénon, and J. Meunier, Phys. Rev. E **54**, 1683 (1996).
[10] S. Rivière, S. Henon, J. Meunier, D. K. Schwartz, M. W. Tsao, and C. M. Knobler, J. Chem. Phys. **101**, 10045 (1994).
[11] S. Ramos and R. Castillo, J. Chem. Phys. **110**, 7021 (1999).
[12] M. M. Lipp, K. Y. C. Lee, D. Y. Takamoto, J. A. Zasadzinski, and A. J. Waring, Phys. Rev. Lett. **81**, 1650 (1998).
[13] H. E. Ries, Nature (London) **281**, 287 (1979).
[14] J. P. Kampf, C. W. Frank, E. E. Malmström, and C. J. Hawker, Science **283**, 1730 (1999).
[15] D. Höning and D. Möbius, J. Phys. Chem. **95**, 4590 (1991).
[16] S. Henon and J. Meunier, Rev. Sci. Instrum. **62**, 936 (1991).
[17] D. Vollhardt and U. Retter, J. Phys. Chem. **95**, 3723 (1991).
[18] D. Vollhardt and U. Retter, Langmuir **8**, 309 (1992).
[19] J. D. Jackson, *Classical Electrodynamics*, 2nd ed. (Wiley, New York, 1975), p. 441.
[20] B. E. A. Saleh and M. C. Teich, *Fundamentals of Photonics* (Wiley, New York, 1991), p. 966.
[21] W. R. Schief, S. B. Hall, and V. Vogel, Phys. Rev. E **62**, 6831 (2000).
[22] C. Lautz, Th. Fischer, M. Weygand, M. Lösche, P. B. Howes, and K. Kjaer, J. Chem. Phys. **108**, 4640 (1998).